Materials Horizons

COMMUNICATION

View Article Online
View Journal | View Issue

Cite this: *Mater. Horiz.*, 2019, 6, 1868

Received 8th January 2019,
Accepted 22nd May 2019

DOI: 10.1039/c9mh00035f

rsc.li/materials-horizons

Design and synthesis of two-dimensional covalent organic frameworks with four-arm cores: prediction of remarkable ambipolar charge-transport properties†

Simil Thomas,‡[a] Hong Li,‡[a] Raghunath R. Dasari,‡[a] Austin M. Evans,[b] Ioannina Castano,[b] Taylor G. Allen,[c] Obadiah G. Reid,[cd] Garry Rumbles,[cd] William R. Dichtel,[b] Nathan C. Gianneschi,[bef] Seth R. Marder,*[a] Veaceslav Coropceanu*[a] and Jean-Luc Brédas*[a]

We have considered three two-dimensional (2D) π-conjugated polymer network (*i.e.*, covalent organic frameworks, COFs) materials based on pyrene, porphyrin, and zinc-porphyrin cores connected *via* diacetylenic linkers. Their electronic structures, investigated at the density functional theory global-hybrid level, are indicative of valence and conduction bands that have large widths, ranging between 1 and 2 eV. Using a molecular approach to derive the electronic couplings between adjacent core units and the electron-vibration couplings, the three π-conjugated 2D COFs are predicted to have ambipolar charge-transport characteristics with electron and hole mobilities in the range of 65–95 $cm^2 V^{-1} s^{-1}$. Such predicted values rank these 2D COFs among the highest-mobility organic semiconductors. In addition, we have synthesized the zinc-porphyrin based 2D COF and carried out structural characterization *via* powder X-ray diffraction, high-resolution transmission electron microscopy, and surface area analysis, which demonstrates the feasibility of these electroactive networks. Steady-state and flash-photolysis time-resolved microwave conductivity measurements on the zinc-porphyrin COF point to appreciable, broadband photoconductivity while transmission spectral measurements are indicative of extended π-conjugation.

New concepts

Two-dimensional fully π-conjugated covalent organic frameworks (COFs) represent an emerging class of materials with rich chemistry and physics. Up to now, the charge-carrier mobility within a single, isolated layer of such COFs had not been characterized. Here, we show theoretically that the mobility in these systems can be described on the basis of concepts similar to those applied to organic mixed-valence systems and can potentially reach values higher than in the best organic crystalline semiconductors. We emphasize the importance of considering properly the electron-vibration couplings that play an important role in all π-conjugated organic materials (a feature however overlooked in earlier reports). We also demonstrate the synthetic feasibility of some of these promising materials. Overall, we expect our work to trigger further experimental and theoretical investigations of these fascinating systems.

1. Introduction

Two-dimensional (2D) materials are garnering a great deal of attention due to their remarkable physical and chemical properties and their high potential for a variety of applications.[1–4] While graphene, the prototypical 2D material, displays electron and hole mobilities in excess of 5000 $cm^2 V^{-1} s^{-1}$ at room temperature,[5] its semimetallic nature prevents its use in many electronic applications.[6] More recently, other 2D materials based on transition metal dichalcogenides have been developed; these systems have a finite bandgap and charge-carrier mobilities up to 200 $cm^2 V^{-1} s^{-1}$ have been reported in the case of MoS_2[7] and WSe_2.[8]

Covalent organic frameworks (COFs) represent another class of promising materials.[9–15] These are porous systems formed by the precise linkage of organic building blocks through covalent bonds in order to generate predetermined assemblies, which

[a] *School of Chemistry and Biochemistry, Center for Organic Photonics and Electronics (COPE), Georgia Institute of Technology, Atlanta, Georgia 30332-0400, USA. E-mail: jean-luc.bredas@chemistry.gatech.edu, marder.seth@chemistry.gatech.edu, coropceanu@gatech.edu*
[b] *Department of Chemistry, Northwestern University, Evanston, Illinois 60208, USA*
[c] *National Renewable Energy Laboratory, 15013 Denver West Parkway, Golden, Colorado 80401, USA*
[d] *Renewable and Sustainable Energy Institute, Department of Chemistry, University of Colorado, Boulder, CO 80309, USA*
[e] *Department of Materials Science and Engineering, Northwestern University, Evanston, IL 60208, USA*
[f] *Department of Biomedical Engineering, Northwestern University, Evanston, IL 60208, USA*

† Electronic supplementary information (ESI) available. See DOI: 10.1039/c9mh00035f

‡ These authors contributed equally.

can have a three-dimensional (3D)[10] or 2D layered structure.[9] Promising applications of COFs include gas storage,[16,17] gas separation,[18] energy storage,[19] catalysis,[20,21] or optoelectronic devices.[14] To date, the measurements of charge-carrier mobilities have been restricted to bulk COF structures.[22] Also, pressed pellets of the fully π-conjugated pyrene-based COF synthesized by Jiang and co-workers show conductivities along the stacks on the order of 7×10^{-4} S cm^{-1} after doping with iodine.[15] In such systems, charge transport can be theoretically described with approaches similar to those used for organic molecular crystals.[23] Up to now, however, except for a few preliminary studies,[24,25] there has been no comprehensive investigation of the charge-transport mechanism within the plane of 2D (isolated) π-conjugated COF sheets. Here, our objective is to develop a theoretical framework to describe charge transport in strictly 2D π-conjugated polymer networks. Our description exploits intra-molecular electron transfer theory,[26] which we have extensively applied earlier in the context of organic mixed-valence systems. 2D COF structures are generally designed on the basis of three-arm cores (for instance, benzene or triphenylene) or four-arm cores (for instance, pyrene or porphyrins). Three-arm cores turn out to have the propensity to lead to the formation of highly symmetric (kagome-like) lattices,[27] which often result in the appearance of totally flat top valence bands and/or bottom conduction bands; in such cases, the charge-carrier effective masses are extremely large and the related carrier mobilities vanish. Thus, we have chosen to work here with four-arm cores.

Given our earlier experience with quasi-1D polypyrene[28] and polyporphyrin[29] conjugated chains and the experimental interest in pyrene and porphyrin 2D COFs, we investigate three 2D conjugated polymer networks based on four-arm pyrene (Pyr-COF), porphyrin (Por-COF), and zinc porphyrin (ZnPor-COF) cores; these are connected *via* diacetylenic linkers, which are selected since they are expected to provide larger electronic couplings between adjacent core units than the typical long, twisted (phenylene-based) linkers.[25,30,31] In addition, sp^2-carbon-conjugated COFs exhibit a higher degree of conjugation with respect to imine-linked COFs. This comes, however, at the expense of a highly difficult synthesis of crystalline, ordered COFs, due to the irreversible nature of C–C coupling chemistry.[15,32–36] The chemical structures of the three 2D COFs under investigation are shown in Fig. 1. We note that the synthesis of Pyr-COF has been recently reported, with powder conductivity measurements giving an electrical conductivity on the order of 10^{-5} S cm^{-1}.[33]

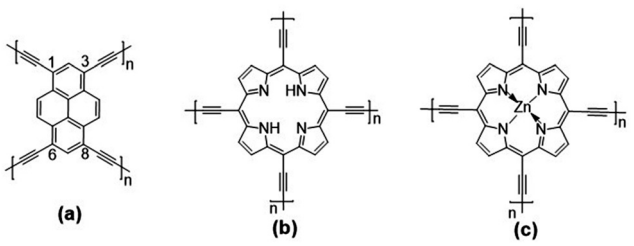

Fig. 1 Chemical structures of the: (a) pyrene (Pyr-COF); (b) porphyrin (Por-COF); and (c) zinc porphyrin (ZnPor-COF) 2D COFs.

In this work, we first combined density functional theory (DFT) calculations with an oligomer approach to estimate the charge-transport parameters. In view of the strength of the connection between the electronic structure and geometric structure in π-conjugated systems,[37] we then evaluated the charge-carrier mobilities by taking explicit account of electron-vibration couplings. We synthesized the Zn-Por COF and, with the insight from the theoretical calculations, carried out: (i) its structural characterization *via* IR, transmission spectral measurements, solid-state ^{13}C NMR, powder X-ray diffraction (PXRD), high-resolution transmission electron microscopy (HR-TEM), and Brunauer–Emmett–Teller (BET) surface area analysis; and (ii) its charge-transport characterization *via* steady-state and flash-photolysis time-resolved microwave conductivity (fp-TRMC) measurements.

2. Computational methodology

The geometry optimizations of the 2D periodic structures were performed at the density functional theory (DFT) level with the global-hybrid PBE0 functional and the POB-TZVP basis set (optimized for periodic solid-state calculations),[38] using a 5×5 *k*-point mesh. During the optimizations, both the atomic positions and the unit-cell parameters were fully relaxed. The electronic band structures were calculated at the same level of theory. The effective masses were evaluated by diagonalizing the inverse of the effective mass tensor ($1/m_{ij}$); the latter was obtained from the valence band maximum or conduction band minimum using a finite-difference method with a 0.01 1/Bohr step. All these calculations were performed with the CRYSTAL17 package.[39,40] The electronic couplings and electron-vibration (phonon) couplings were evaluated from the energies of the ground and excited states of molecular fragments, as discussed below. All molecular electronic-structure calculations were performed with the PBE0 functional and the 6-31G(d,p) basis set, using the Gaussian 09 package.[41]

3. Results and discussion

3.1. Geometric and electronic structure

The unit cell of Pyr-COF contains four ethynylene linkers that are connected to the 1, 3, 6, and 8 positions of a pyrene core, as illustrated in Fig. 1(a). The optimized Pyr-COF lattice symmetry belongs to the *p2gg* plane group (characterized by glide reflection symmetry), with unit-cell parameters $a_1 = a_2 = 12.08$ Å and $\gamma = 96^\circ$. In both Por-COF and ZnPor-COF, the four ethynylene linkers are connected to the *meso* positions of the porphyrin or zinc porphyrin cores, see Fig. 1(b) and (c). The optimized unit-cell parameters of the Por-COF and ZnPor-COF are $a_1 = a_2 = 13.44$ Å and $\gamma \approx 90^\circ$, and $a_1 = a_2 = 13.43$ Å and $\gamma \approx 90^\circ$, respectively. Assuming that in Pyr-COF the two hydrogens effectively delocalize among the four inner N atoms, both systems belong to the *p4mm* plane group (characterized by reflection symmetry with mirrors at 45°). The band structures of the three COFs are shown in Fig. 2. They are direct-gap

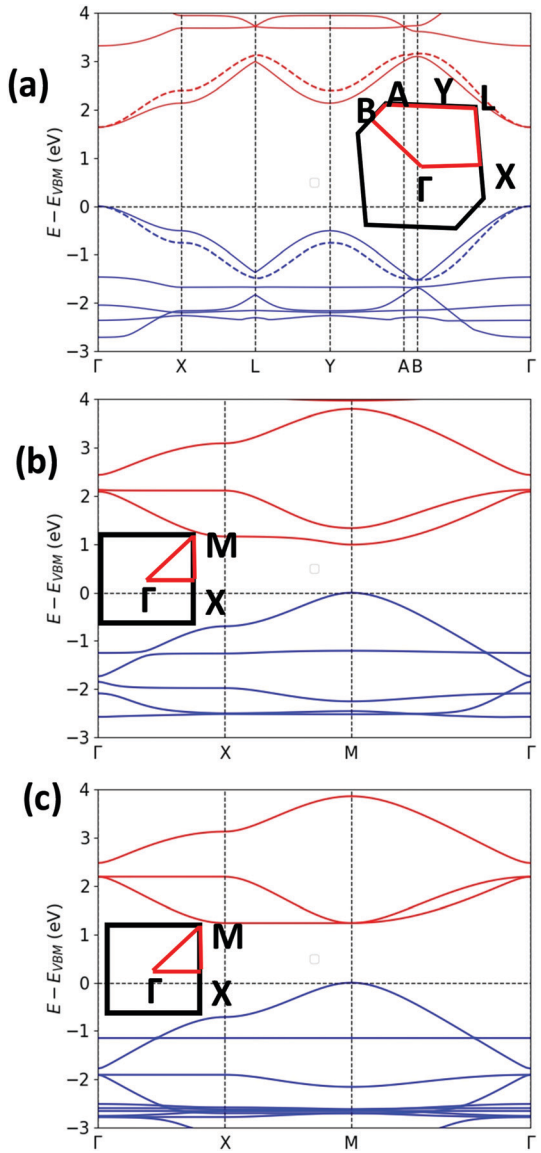

Fig. 2 DFT-PBE0-calculated electronic band structures of: (a) Pyr-COF (the two bands depicted with dashed lines refer to those derived from the tight-binding modelling); (b) Por-COF; and (c) ZnPor-COF (the Brillouin zones and high-symmetry points are shown in the insets). The valence and conduction bands are colored in blue and red, respectively. The zero of energy is taken as the valence band maximum, E_{VBM} (shown by the horizontal dashed gray line).

semiconductors with calculated bandgaps of 1.63 eV (at the Γ-point) for Pyr-COF, 0.99 eV (at the K-point) in Por-COF, and 1.23 eV (at the K-point) in ZnPor-COF. These systems can thus be classified as low bandgap COF materials, which are of current great interest.[42] Importantly, the conduction and valence bands exhibit large widths in all three COFs: 1.5 eV [1.5 eV] for the valence band [conduction band] in Pyr-COF; 1.7 eV [1.1 eV] in Por-COF, and 1.8 eV [1.0 eV] in ZnPor-COF. As a direct result of the strong dispersion of the frontier electronic bands, the effective masses for both holes and electrons are small. Given that the Pyr-COF unit cell is oblique and thus deviates from a square unit cell, the charge-transport properties are expected to be anisotropic; we find indeed effective masses in Pyr-COF of 0.13 m_0 and 0.24 m_0 for holes and 0.12 m_0 and 0.26 m_0 for electrons. In the porphyrin COFs, the hole effective masses are calculated to be even smaller and more isotropic (in view of the quasi-square lattice symmetry): 0.07 m_0 and 0.09 m_0 in Por-COF and 0.08 m_0 and 0.10 m_0 in ZnPor-COF. In the case of electrons, the situation in the porphyrin systems turns out to be more complex due to (quasi-)degeneracy of the LUMO and LUMO+1 orbitals (see ESI†), which results in a strong mixing of the electronic states around the conduction band minimum; this feature is particularly evident in the case of ZnPor-COF where the two corresponding sub-bands are degenerate at the M point. In this instance, in analogy with the case of the valence band in GaAs, it would be necessary to introduce effective masses for each sub-band;[43] since a full account of this issue is beyond the scope of the present work, we simply mention that, based on a fitting of the lowest conduction sub-bands in Por-COF and ZnPor-COF, the electron effective masses are estimated to be as small as *ca.* 0.1 m_0. It is important to emphasize that, overall, such small effective masses are among the lowest calculated for organic-based semiconductors and can be expected to give rise to high charge-carrier mobilities.

3.2. Electronic couplings

As a useful step towards determining the strength of the electronic couplings between adjacent core units, we take Pyr-COF as an example and show next that its electronic structure can be rationalized in the framework of a simple tight-binding, Hückel-like model. Inspection of the 2D-periodic wave functions indicates that the charge transport for both electron and holes can be viewed as originating in electron/hole transfer between adjacent pyrene units, which play the role of charge-carrying moieties. This is more clearly seen when considering the frontier orbitals (see Fig. 3) of a molecular model consisting of two diacetylene-linked pyrene units (to which we refer below as a dimer; see also Fig. S1, ESI†). As illustrated by Fig. 3, the HOMO (highest occupied molecular orbital) and

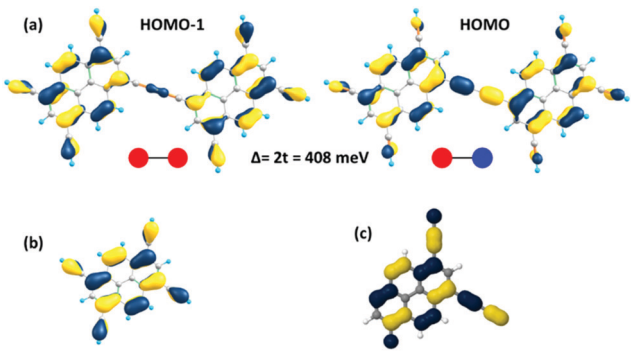

Fig. 3 (a) Illustration of the HOMO−1 and HOMO wavefunctions in the Pyr-COF dimer and estimation of the transfer integrals (t) for holes, based on the energy-splitting approach; Δ denotes the difference between the HOMO and HOMO−1 energies of the dimer; the red and blue dots express the symmetry of the tight-binding wavefunctions. (b) HOMO of the pyrene building block. (c) Wave-function of the valence band maximum of the 2D Pyr-COF at the Γ-point.

HOMO−1 represent symmetric and anti-symmetric linear combinations of the HOMOs of the pyrene units. The same holds true for the LUMO (lowest unoccupied molecular orbital) and LUMO+1, see Fig. S2 (ESI†). It is also useful to note the similarity between the dimer HOMO and the wavefunction of the 2D Pyr-COF at the valence band maximum (Γ-point). Importantly, this picture is strongly reminiscent of that typically found in the case of intra-molecular electron transfer in organic mixed-valence systems.[26] Indeed, since there is no direct overlap between the frontier orbitals of the pyrene cores, the electron transfer between two localized (diabatic) pyrene states is in fact mediated by the linker units, as is usually the case for mixed-valence systems. Thus, the electronic couplings between the (charge-carrying) pyrene moieties has a super-exchange nature and come from the mixing of the pyrene frontier with the diacetylenic linker orbitals. This feature clearly underlines that the choice of both the charge-carrying units and the linkers is critical to secure good charge-transport properties. Taking advantage of the similarity with mixed-valence systems, we can use the energies of the frontier orbitals of the pyrene dimer to estimate the effective electronic couplings, t_{eff}, between adjacent core units by means of the dimer energy-splitting approach:[23,26]

$$t_{\mathrm{eff}} = \frac{E_{\mathrm{H[L+1]}} - E_{\mathrm{H-1[L]}}}{2} \quad (1)$$

where $E_{\mathrm{H[L]}}$ and $E_{\mathrm{H-1[L+1]}}$ are the energies of the HOMO and HOMO−1 [LUMO (and LUMO+1)] levels of the dimer in the 2D COF geometry. We note that, to confirm the validity of this approach, we applied it as well to tetramers and obtained similar results for t_{eff} (see Fig. S2d, ESI†). Since the results based on dimers are more straightforward to discuss, we focus on them below. In Pyr-COF, t_{eff} is *ca.* 204 meV and has the same value for holes and electrons. It must be stressed that such values are much larger than those reported in the case of the organic molecular crystals with the highest charge-carrier mobilities (for example, t_{eff} is estimated to be 85 meV in the pentacene crystal and 83 meV in the rubrene crystal).[23] 2D periodic tight-binding (Hückel) calculations, where we consider one effective orbital energy per site and use the effective transfer integrals coming from the dimer calculations, reproduce very well the DFT-PBE0 valence and conduction bands of Pyr-COF (see the dotted-line frontier electronic bands in Fig. 2a). Also, the bandwidths can be estimated as 8 times t_{eff} (*i.e.*, 1.6 eV), which is as well in very good agreement with the DFT bandwidths (1.5 eV). Even larger transfer integrals, 232 meV, are predicted for holes in both Por-COF and ZnPor-COF (see Fig. S3 and S4, ESI†); there again the tight-binding simulations reproduce very well the DFT valence bands (see Fig. S5 and S6, ESI†). As noted above, the orbital (quasi-)degeneracy between the LUMO and LUMO+1 levels (see Fig. S7 and S8, ESI†) in Por-COF and ZnPor-COF preclude a straightforward application of the dimer approach to estimate the transfer integrals for electrons in these systems. However, the similarity between the calculated effective masses for holes and electrons (see Table S1, ESI†) indicates that the corresponding transfer integrals are also comparable. This conclusion is also supported by the inter-valence charge-transfer data reported for the mixed-valence cation and anion radicals of bis(porphyrinyl)butadiyne (which is a structural analogue to the Zn-Por dimer considered here); the transfer integrals deduced from these experimental data are 225 and 253 meV for electrons and holes, respectively;[44] these values compare extremely well with our 232 meV DFT estimate.

3.3. Electronic-vibration couplings

In addition to the electronic couplings, the characterization of the charge-transport properties also requires the knowledge of the electron-vibration (phonon) couplings. As was shown in the case of organic molecular crystals,[23] there exist two electron-vibration mechanisms that affect charge transport. The first mechanism comes from the vibration-induced modulations of the site energies and is usually referred to as the local electron-vibration coupling; the local coupling is the key interaction accounted for in Holstein-type polaron models[45,46] and Marcus electron-theory;[47] its strength is expressed in terms of the polaron binding energy, E_{pol}, or the reorganization energy, λ (whose value is twice E_{pol}). The local electron-vibration contributions can be evaluated from the energies of the neutral and anion or cation states of the charge-carrying moieties, as discussed in detail elsewhere.[23] The DFT calculations yield E_{pol} values for holes [electrons] of 67 [96] meV, 27 [85] meV, and 28 [47] meV in Pyr-COF, Por-COF, and ZnPor-COF, respectively. Since these E_{pol} values are significantly smaller than the relevant electronic bandwidths, the local electron-vibration interactions are not strong enough to lead to charge-carrier localization and the formation of small (molecular) polarons. The second electron-vibration coupling mechanism is referred to as non-local or Peierls coupling;[23,48] it stems from the modulation of the transfer integrals by vibrational (phonon) modes:

$$t_{\mathrm{eff}} = t_{\mathrm{eff}}^{(0)} + \sum \nu_j Q_j \quad (2)$$

where ν_j and Q_j denote the vibrational coupling constants and coordinates of the vibrational modes, respectively. Since a comprehensive description of this mechanism in 2D COFs still poses a very challenging task, it is useful here as well to take advantage of the dimer approach developed for mixed-valence systems; the strength of the non-local electron-vibration coupling, L (with $L = \sum \nu_j^2/\hbar\omega_j$, where ω_j denotes the frequency of vibrational mode Q_j), can be accessed from the potential energy surfaces of the ground and first excited states of the charged dimers, which have been used for the transfer-integral calculations.[23,26] The L values derived for hole [electron] transport are 48 [49] meV, 76 meV, and 67 meV in Pyr-COF, Por-COF, and ZnPor-COF, respectively. These values are significant and result in substantial modulations of the transfer integrals at elevated temperatures (see Table S2, ESI†). Thus, these results point out that the non-local electron-vibration interactions represent an important scattering mechanism for charge carriers in the 2D systems investigated here.

3.4. Charge-carrier mobilities

In order to estimate the carrier mobilities, the local electron-vibration coupling, being mainly due to high-frequency vibration modes, can be taken to contribute only to a renormalization of the transfer integrals and non-local electron-vibration couplings. Following Zhu *et al.*,[49] the renormalization parameter α corresponds to:

$$\alpha = \exp\{-E_{\mathrm{pol}} \coth(\hbar\omega/2k_{\mathrm{B}}T)/\hbar\omega\} \quad (3)$$

where ω is the frequency of an effective vibration mode. By using a value of ω = 1200 cm^{-1}, representative of carbon–carbon bond stretches in π-conjugated systems, and the E_{pol} values given above, the derived α values are 0.63, 0.83, and 0.83 in Pyr-COF, Por-COF, and ZnPor-COF, respectively. Since the ratio $L/t = \zeta$ is in all cases smaller than 1 (ζ = 0.24 in Pyr-COF, 0.29 in Por-COF, and 0.32 in ZnPor-COF), which means that the electronic couplings are significantly stronger than the electron-vibration couplings, the carrier mobilities can be evaluated by considering that charge transport takes place in the band regime and treating the non-local coupling as a perturbation (relaxation-time approximation).[50]

The mobilities along the [10] and [01] directions can then be calculated by means of eqn (4), which has originally been derived for a one-dimensional case in the limit where the bandwidth is much larger than $k_{\mathrm{B}}T$, which is the case here:[50,51]

$$\mu_{\mathrm{band}} = \frac{ea^2}{\hbar}\frac{1}{8\sqrt{\pi}\zeta}\left(\frac{t}{k_{\mathrm{B}}T}\right)^{\frac{3}{2}} \quad (4)$$

In eqn (4), a denotes the distance between two adjacent core units. Taking into account the (renormalization) effect of the local electron-vibration interactions, the mobilities are estimated to fall in a range from *ca.* 66 $\mathrm{cm}^2\ \mathrm{V}^{-1}\ \mathrm{s}^{-1}$ for both electrons and holes in Pyr-COF, to *ca.* 82 $\mathrm{cm}^2\ \mathrm{V}^{-1}\ \mathrm{s}^{-1}$ and 94 $\mathrm{cm}^2\ \mathrm{V}^{-1}\ \mathrm{s}^{-1}$ for holes in Por-COF and ZnPor-COF, respectively (see Table S3, ESI,† where we also list the mobility values when the renormalization due to the local electron-vibration coupling is neglected). These mobility values are of the same order of magnitude as those experimentally measured in graphdiyne (up to 100 $\mathrm{cm}^2\ \mathrm{V}^{-1}\ \mathrm{s}^{-1}$), where benzene cores are connected *via* six diacetylenic linkers.[52]

Finally, we note that we also calculated the mobilities by treating the electron-vibration couplings in the framework of the deformation potential (DP)[53] model (see ESI,† for details). The reason is that this model has been recently used to estimate the mobilities in single-layer Hittorf's phosphorus,[54] graphene,[55] graphdiyne sheets,[56] and triangulene-based COF.[57] The DP-based mobilities (see Table S4, ESI†) are calculated to reach nearly 8×10^3 $\mathrm{cm}^2\ \mathrm{V}^{-1}\ \mathrm{s}^{-1}$ for both holes and electrons in Pyr-COF and are even one order of magnitude larger in Por-COF. These results underline that the charge-carrier scattering due to the DP mechanism plays only a minor role on the charge-transport properties of the 2D COFs investigated here; thus, given the propensity of the DP model to hugely overestimate the mobilities of π-conjugated 2D COFs, its application to such systems should be made with much caution.[57]

3.5. Synthesis and characterization of ZnPor-COF

To demonstrate that these diacetylene-linked porphyrin COF materials can be realized, the zinc-metallated porphyrin 2D COF, ZnPor-COF, **2**, was synthesized by copper-catalyzed Eglinton coupling of the 5,10,15,20-tetrakis(ethynyl)porphyrin-zinc(II) monomer, **1**, ZnTEP, which was itself synthesized according to literature procedures,[58,59] see Fig. 4A and the ESI,† for more details. We note that the metal-free porphyrin COF, Por-COF, could not be synthesized due to the insolubility of the ZnTEP monomer in common organic solvents.

To evaluate whether the ZnPor-COF synthesis conditions created a crystalline network, we collected powder X-ray diffraction (PXRD) patterns of the resultant materials. The optimized reaction conditions yielded **2** as a micro-crystalline solid, as indicated by its PXRD pattern (Fig. 4C). A diffraction feature was observed at approximately two theta = 7.5°, which we assigned to the approximate spacing between Zn atoms and the 100 Bragg peak. This, combined with the geometric constraints of the monomers, indicated to us that the 2D structure was that shown in Fig. 4B. We thus modelled the structure

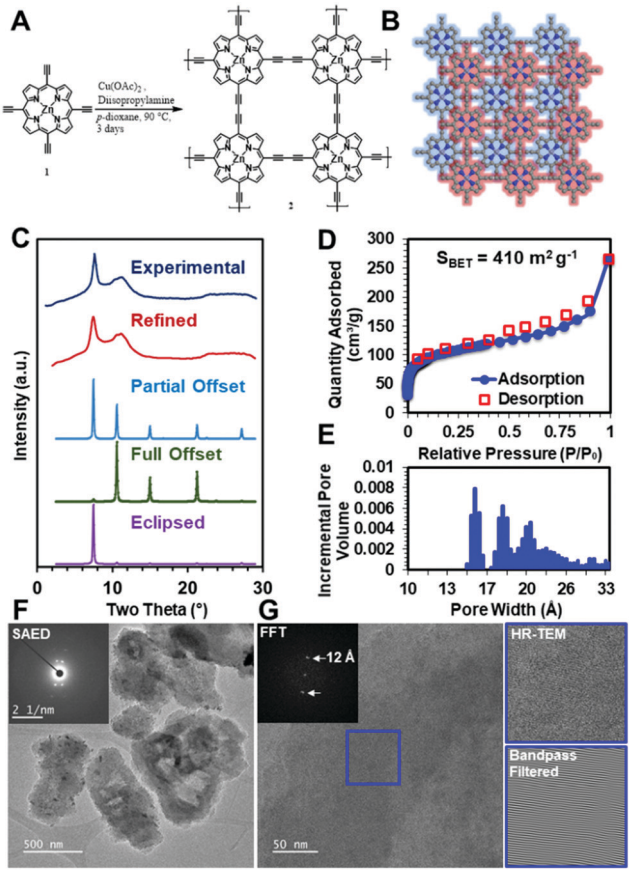

Fig. 4 (A) Synthesis of zinc porphyrin 2D COF; (B) modelled porphyrin COF structure; (C) experimental and simulated PXRD patterns; (D) N_2 adsorption (closed circles) and desorption (open squares) isotherms (77 K) for **2**, and (E) pore size distribution of **2**. (F) Low-resolution TEM image (inset: SAED pattern of particles) (G) high-resolution TEM image (inset: FFT of boxed region in (G). Side panels: lattice image of boxed region in (G) and bandpass filtered image of that region) of zinc porphyrin 2D COF particles.

using a primitive P4 unit cell. However, we were also interested in assigning the stacking structure of the 2D sheets. We first modelled the stacking of a completely eclipsed (AA stacking) and completely offset structure (AB stacking), which we then used to predict their respective XRD patterns (Fig. 4C). The relative intensities of the 100 and 110 features indicated that the stacking was between fully eclipsed and fully offset. Using this information, we conducted a Pawley refinement to more appropriately determine the correct structure. This produced a partially offset structure with a predicted diffraction pattern in good agreement with the experimentally obtained patterns (Fig. 4C). We then allowed the predicted pattern to broaden due to finite-grain effects (details available in the ESI†). This analysis indicates that the crystallites have an average in-plane dimension of 30 nm, which is consistent with previously reported COFs.[60] To assess the extent of functional group conversion, we collected the attenuated total reflectance-infrared spectrum of **2**, and compared with the tetraethynylzinc-porphyrin monomer **1** spectrum in Fig. S9a, see ESI.† The characteristic terminal alkyne C–H stretch at 3269 cm^{-1} of monomer **1** is absent in **2**, indicating consumption of terminal acetylene of **1**. The alkyne CC vibration at 2087 cm^{-1} of **1** was observed at 2150 cm^{-1} in **2**. Similar shifts in alkyne CC vibration peaks were observed for the diphenylbutadiyne[61] model compound, which was synthesized using the same synthesis conditions as for the COF, see Fig. S9b in ESI.† Solid-state CP/MAS ^{13}C NMR of **2** show three resonances related to the porphyrin ring, and two weak resonances are attributed to the acetylene moiety at 85.4 and 74.3 ppm (Fig. S9c, ESI†). However, the appearance of resonances at 49.1 and 20.7 ppm suggest that trace amounts of diisopropylamine, which was used as a base in the COF synthesis, might present in COF **2** sample pores. To more fully characterize the structure of the COF material, we performed N_2 isotherm experiments and a Brunauer–Emmett–Teller (BET) analysis to determine the surface area and pore size distribution of this COF (Fig. 4D and E). This measurement shows that the COF has a high surface area of >400 m^2 g^{-1}, to be compared with a theoretical surface area of 900 m^2 g^{-1}, see ESI,† for details; this deviation in surface area from the theoretical value is typical for microcrystalline COF powders. Moreover, the contaminants in the COF sample, as confirmed by solid-state ^{13}C NMR, may have contributed to the observed lower surface area values. Additionally, the pore size distribution shows a maximum at approximately 1 nm, which is consistent with expected pore size of the offset structure. However, the broad XRD features, lower than ideal surface area, and broad pore size distributions indicate that defects are present within the material. To investigate the Zn-porphyrin material structure further, we imaged the COF using high-resolution transmission electron microscopy (HR-TEM). The low-resolution images in Fig. 4F show that the crystallites are unfaceted sheet-like particles of approximately one-micron length. Selected-area electron diffraction (SAED) (Fig. 4F inset) of the particles resulted in a four-fold diffraction pattern consistent with the spacing observed by bulk XRD. High-resolution images (Fig. 4G) of the same crystallites showed lattice fringes of approximately 1.2 nm, which were more easily seen when the image was bandpass filtered, further substantiating the structural assignment of the offset layers. Additional TEM images of ZnPor-COF are presented Fig. S10 and S11 (ESI†).

fp-TRMC measurements[62,63] were performed on ZnPor-COF and monomer-like ([5,10,15,20-tetraphenylporphyrinato]zinc(II), ZnTPP) films to obtain an estimate of the mobilities for both materials. In doing so, we seek to deduce empirically the extent of delocalization in ZnPor-COF relative to ZnTPP. To facilitate measurements, the insoluble ZnPor-COF powder was embedded in inert polymer hosts (poly(methyl methacrylate), PMMA) or polystyrene (PS), (see ESI† for film processing details) to afford films with complete surface coverage of the substrate. Analysis of the AC mobilities obtained by fp-TRMC for crystalline particles is usually done with the Kubo relation,[64,65] which requires as input the crystallite size. Taking for ZnPor-COF the crystallite size (30 nm) measured by PXRD and assuming the intrinsic (large-scale) mobility predicted theoretically (90 cm^2 V^{-1} s^{-1}), the Kubo relation gives 3.5×10^{-2} cm^2 V^{-1} s^{-1} as the maximum AC mobility that could be measured at 9 GHz for such particle sizes (Fig. S12, ESI†). Upon photoexcitation at 700 nm of the ZnPor-COF–polymer films, the fp-TRMC measurements provide a yield-mobility product ($\phi\Sigma\mu$) of *ca.* 3×10^{-5} cm^2 V^{-1} s^{-1}. This experimental value of the yield-mobility product combined with the theoretical estimate of the maximum AC mobility allows us to place limits on both the actual charge carrier yield and the AC mobility. The former may range from 100–0.1%, and the latter from 3×10^{-5}–3.5×10^{-2} cm^2 V^{-1} s^{-1} (see Fig. 5 and Fig. S13–S15, ESI†). There is no reasonable expectation that every photon would generate a pair of charges (100% yield); thus, the AC mobility is likely in the upper end of the estimated range. Since neat conjugated polymers rarely exhibit charge yields above 10%,[66–68] this suggests that the AC mobility within ZnPor-COF 30 nm crystallites should be over 10^{-4} cm^2 V^{-1} s^{-1}.

fp-TRMC measurements on a neat film of the monomer-like ZnTPP upon excitations at 430, 550, and 700 nm – *i.e.*, on resonance with the Soret (430 nm) and Q-band (550 nm)

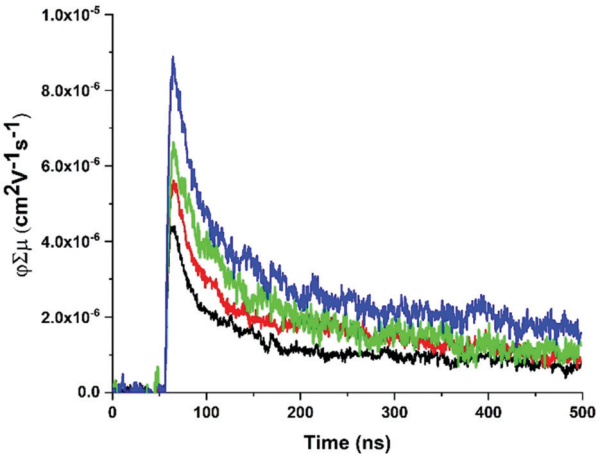

Fig. 5 Representative fp-TRMC transients with increasing fluence (1×10^{14}–4×10^{15} photons per cm^2) for a ZnPor-COF-PS film at 700 nm photoexcitation with 7 ns pulse width.

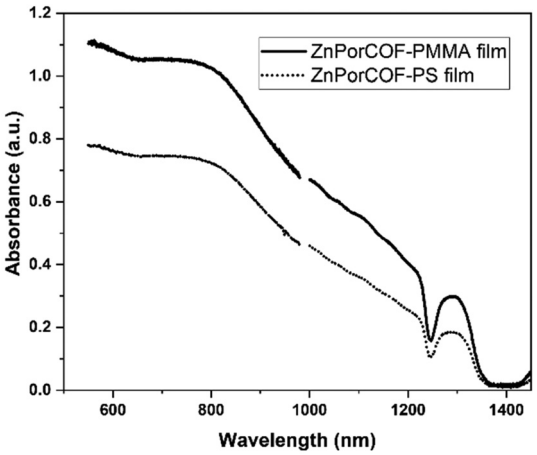

Fig. 6 Absorption spectra for ZnPor-COF–polymer blends taken by integrating sphere, without scattering contributions. (We note that the lamp output ends at *ca.* 1400 nm; the dip at 1250 nm is likely related to overtone absorption losses by the optical fiber carrying the source light).

transitions, and off-resonance at 700 nm – did not result in measurable yield-mobility products, see Fig. S16 (ESI†). The generation of photocarriers at 700 nm in ZnPorCOF–polymer films, far from typical Zn-porphyrin monomer resonances, is thus indicative of delocalized excitations due to electronic couplings among Zn porphyrin units in the COF. This is corroborated by the absorption spectra (acquired *via* transmission measurements) of ZnPor-COF–polymer films that show considerable optical density over the range of 300–1800 nm relative to the more discrete spectrum of ZnTPP (Fig. S17, ESI†). We note that, to rule out scattering contributions, absorption spectra of ZnPorCOF–polymer films were collected using an integrating sphere; these spectra also show extended absorption over the visible-to-NIR range, see Fig. 6.

In support of these data, photoconductivity action spectra were acquired by a steady-state microwave conductivity experiment (see ESI,† for details). Like the absorption spectra of ZnPor-COF–polymer films, the action spectra showed broadband photoconductivity over the range of 600–1100 nm (Fig. S18 and S19, ESI†), which is consistent with the band structures calculated in Section 3.1. Akin to fp-TRMC measurements, neat ZnTPP did not afford measurable steady-state photoconductivity over a wavelength range of 400–750 nm.

4. Conclusions

We have investigated at the DFT-PBE0 level the electronic structure of 2D π-conjugated polymer networks based on four-arm pyrene, porphyrin, and zinc porphyrin cores connected *via* diacetylenic linkers. The three 2D COFs are characterized by large widths of both valence and conduction bands, on the order of 1.5 to 2 eV, which leads to small hole and electron effective masses. Our work demonstrates that the charge-transport properties of these 2D polymer networks, based on fully π-conjugated core and linker building blocks, can be described by models akin to those used to characterize electron transfer in organic mixed-valence systems. Thus, calculations on fragments extracted from 2D COF structures can provide simple (and quick) estimates of the electronic and electron-vibration couplings. Our approach can therefore be used for screening the potential mobility values in new materials, even though more extended first-principles calculations of the electron-vibration (phonon) couplings could provide a more comprehensive description of the charge-transport properties in π-conjugated COFs. Considering the impact of (local and nonlocal) electron-vibration couplings, remarkable charge-carrier mobility values in the 65–95 $cm^2\ V^{-1}\ s^{-1}$ range are predicted for both electrons and holes in the 2D COFs investigated here. These rank among the largest values, predicted and measured, in organic (macro-) molecular semiconductors.

A COF network consisting of four-arm zinc porphyrin cores was synthesized. We obtained a micro-crystalline structure, which based on the correlation between the experimental and simulated PXRD patterns, nitrogen isotherms, and electron microscopy, shows the expected tessellated structure. Steady-state and time-resolved microwave conductivity measurements reveal appreciable, broadband photoconductivity for ZnPor-COF whereas monomer-like ZnTPP shows no measurable mobilities. The next, challenging steps are to develop experimental protocols that will both enable the formation of COF with larger grain sizes and allow for exfoliation of the 2D sheets and direct characterization of their intrinsic charge-transport properties. Our joint theoretical and experimental study points to important new directions for the development of COFs with exceptional electronic properties.

Conflicts of interest

There are no conflicts to declare.

Acknowledgements

J. L. B., S. R. M. and W. R. D. acknowledge the United States Army Research Office for a Multidisciplinary University Research Initiative (MURI) award under grant number W911NF-15-1-0447. A. M. E. is supported by the National Science Foundation Graduate Research Fellowship under Grant No. (DGE-1324585). I. C. is supported by the Ryan Fellowship and the Northwestern University International Institute for Nanotechnology. V. C. acknowledges support by the National Science Foundation (DMR-1708147). We thank Vamsi Krishna Narra, Cameron Feriante, Johannes E. Leisen, and Ruhui Chen for help with synthesis, PXRD, solid-state NMR, and ICP-MS measurements, respectively. We are grateful to Timothy C. Parker for helpful discussions. This work has also made use of the EPIC facility of NUANCE Center at Northwestern University, which has received support from the Soft and Hybrid Nanotechnology Experimental (SHyNE) Resource (NSF ECCS-1542205), the MRSEC program (NSF DMR-1720139) at the Materials Research Center, the Keck Foundation, the State of Illinois and International Institute for

Nanotechnology (IIN). This work was authored by the National Renewable Energy Laboratory, operated by Alliance for Sustainable Energy, LLC, for the U.S. Department of Energy (DOE) under Contract No. DE-AC36-08GO28308. Funding for microwave measurements provided by Department of Energy, Office of Basic Energy Sciences, Division of Chemical Sciences, Biosciences, and Geosciences. The views expressed in the article do not necessarily represent the views of the DOE or the U.S. Government. The U.S. Government retains and the publisher, by accepting the article for publication, acknowledges that the U.S. Government retains a nonexclusive, paid-up, irrevocable, worldwide license to publish or reproduce the published form of this work, or allow others to do so, for U.S. Government purposes.

Notes and references

1 M. C. Lemme, L.-J. Li, T. Palacios and F. Schwierz, *MRS Bull.*, 2014, **39**, 711–718.
2 K. I. Bolotin, K. J. Sikes, Z. Jiang, M. Klima, G. Fudenberg, J. Hone, P. Kim and H. L. Stormer, *Solid State Commun.*, 2008, **146**, 351–355.
3 Z. Yin, H. Li, H. Li, L. Jiang, Y. Shi, Y. Sun, G. Lu, Q. Zhang, X. Chen and H. Zhang, *ACS Nano*, 2012, **6**, 74–80.
4 G. R. Bhimanapati, Z. Lin, V. Meunier, Y. Jung, J. Cha, S. Das, D. Xiao, Y. Son, M. S. Strano, V. R. Cooper, L. Liang, S. G. Louie, E. Ringe, W. Zhou, S. S. Kim, R. R. Naik, B. G. Sumpter, H. Terrones, F. Xia, Y. Wang, J. Zhu, D. Akinwande, N. Alem, J. A. Schuller, R. E. Schaak, M. Terrones and J. A. Robinson, *ACS Nano*, 2015, **9**, 11509–11539.
5 A. S. Mayorov, R. V. Gorbachev, S. V. Morozov, L. Britnell, R. Jalil, L. A. Ponomarenko, P. Blake, K. S. Novoselov, K. Watanabe, T. Taniguchi and A. K. Geim, *Nano Lett.*, 2011, **11**, 2396–2399.
6 F. Xia, D. B. Farmer, Y.-m. Lin and P. Avouris, *Nano Lett.*, 2010, **10**, 715–718.
7 B. Radisavljevic, A. Radenovic, J. Brivio, V. Giacometti and A. Kis, *Nat. Nanotechnol.*, 2011, **6**, 147.
8 Q. H. Wang, K. Kalantar-Zadeh, A. Kis, J. N. Coleman and M. S. Strano, *Nat. Nanotechnol.*, 2012, **7**, 699.
9 A. P. Côté, A. I. Benin, N. W. Ockwig, M. O'Keeffe, A. J. Matzger and O. M. Yaghi, *Science*, 2005, **310**, 1166–1170.
10 H. M. El-Kaderi, J. R. Hunt, J. L. Mendoza-Cortés, A. P. Côté, R. E. Taylor, M. O'Keeffe and O. M. Yaghi, *Science*, 2007, **316**, 268–272.
11 F. J. Uribe-Romo, J. R. Hunt, H. Furukawa, C. Klöck, M. O'Keeffe and O. M. Yaghi, *J. Am. Chem. Soc.*, 2009, **131**, 4570–4571.
12 X. Feng, X. Ding and D. Jiang, *Chem. Soc. Rev.*, 2012, **41**, 6010–6022.
13 J. W. Colson and W. R. Dichtel, *Nat. Chem.*, 2013, **5**, 453.
14 M. Dogru and T. Bein, *Chem. Commun.*, 2014, **50**, 5531–5546.
15 E. Jin, M. Asada, Q. Xu, S. Dalapati, M. A. Addicoat, M. A. Brady, H. Xu, T. Nakamura, T. Heine, Q. Chen and D. Jiang, *Science*, 2017, **357**, 673–676.
16 H. Furukawa and O. M. Yaghi, *J. Am. Chem. Soc.*, 2009, **131**, 8875–8883.
17 Z. Yongfei, Z. Ruqiang and Z. Yanli, *Adv. Mater.*, 2016, **28**, 2855–2873.
18 S. Kandambeth, B. P. Biswal, H. D. Chaudhari, K. C. Rout, S. K. H, S. Mitra, S. Karak, A. Das, R. Mukherjee, U. K. Kharul and R. Banerjee, *Adv. Mater.*, 2017, **29**, 1603945.
19 D. Ya, Y. Haishen, W. J. Michael, W. Shun, J. Yinghua, L. Se-Hee and Z. Wei, *Angew. Chem., Int. Ed.*, 2016, **55**, 1737–1741.
20 S.-Y. Ding, J. Gao, Q. Wang, Y. Zhang, W.-G. Song, C.-Y. Su and W. Wang, *J. Am. Chem. Soc.*, 2011, **133**, 19816–19822.
21 H. Li, Q. Pan, Y. Ma, X. Guan, M. Xue, Q. Fang, Y. Yan, V. Valtchev and S. Qiu, *J. Am. Chem. Soc.*, 2016, **138**, 14783–14788.
22 D. Xuesong, G. Jia, F. Xiao, H. Yoshihito, G. Jingdong, S. Shu, M. Phornphimon, S. Akinori, N. Shigeru and J. Donglin, *Angew. Chem., Int. Ed.*, 2011, **50**, 1289–1293.
23 V. Coropceanu, J. Cornil, D. A. da Silva Filho, Y. Olivier, R. Silbey and J.-L. Brédas, *Chem. Rev.*, 2007, **107**, 926–952.
24 V. Laszlo and T. Kowalczyk, *J. Mater. Chem. A*, 2016, **4**, 10500–10507.
25 V. Posligua, A. Aziz, R. Haver, M. D. Peeks, H. L. Anderson and R. Grau-Crespo, *J. Phys. Chem. C*, 2018, **122**, 23790–23798.
26 V. Coropceanu, M. Malagoli, J. M. André and J. L. Brédas, *J. Am. Chem. Soc.*, 2002, **124**, 10519–10530.
27 S. Thomas, H. Li, C. Zhong, M. Matsumoto, W. R. Dichtel and J.-L. Bredas, *Chem. Mater.*, 2019, **31**, 3051–3065.
28 J. M. Toussaint, F. Wudl and J. L. Brédas, *J. Chem. Phys.*, 1989, **91**, 1783–1788.
29 D. Beljonne, G. E. O'Keefe, P. J. Hamer, R. H. Friend, H. L. Anderson and J. L. Brédas, *J. Chem. Phys.*, 1997, **106**, 9439–9460.
30 B. Sun, C.-H. Zhu, Y. Liu, C. Wang, L.-J. Wan and D. Wang, *Chem. Mater.*, 2017, **29**, 4367–4374.
31 H. Liao, H. Wang, H. Ding, X. Meng, H. Xu, B. Wang, X. Ai and C. Wang, *J. Mater. Chem. A*, 2016, **4**, 7416–7421.
32 X. Zhuang, W. Zhao, F. Zhang, Y. Cao, F. Liu, S. Bi and X. Feng, *Polym. Chem.*, 2016, **7**, 4176–4181.
33 P. Prabakaran, S. Satapathy, E. Prasad and S. Sankararaman, *J. Mater. Chem. C*, 2018, **6**, 380–387.
34 E. Jin, J. Li, K. Geng, Q. Jiang, H. Xu, Q. Xu and D. Jiang, *Nat. Commun.*, 2018, **9**, 4143.
35 S. Wu, M. Li, H. Phan, D. Wang, T. S. Herng, J. Ding, Z. Lu and J. Wu, *Angew. Chem., Int. Ed.*, 2018, **57**, 8007–8011.
36 Y. Zhao, H. Liu, C. Wu, Z. Zhang, Q. Pan, F. Hu, R. Wang, P. Li, X. Huang and Z. Li, *Angew. Chem., Int. Ed.*, 2019, **58**, 5376–5381.
37 J. L. Bredas and G. B. Street, *Acc. Chem. Res.*, 1985, **18**, 309–315.
38 M. F. Peintinger, D. V. Oliveira and T. Bredow, *J. Comput. Chem.*, 2013, **34**, 451–459.
39 R. Dovesi, V. R. Saunders, C. Roetti, R. Orlando, C. M. Zicovich-Wilson, F. Pascale, B. Civalleri, K. Doll, N. M. Harrison, I. J. Bush, P. D'Arco, M. Llunell, M. Causà, Y. Noël, L. Maschio, A. Erba, M. Rerat and S. Casassa, *CRYSTAL17 User's Manual*, University of Torino: Torino, 2017.

40 R. Dovesi, A. Erba, R. Orlando, C. M. Zicovich-Wilson, B. Civalleri, L. Maschio, M. Rérat, S. Casassa, J. Baima, S. Salustro and B. Kirtman, *Wiley Interdiscip. Rev.: Comput. Mol. Sci.*, 2018, **8**, e1360.
41 M. J. Frisch, G. W. Trucks, H. B. Schlegel, G. E. Scuseria, M. A. Robb, J. R. Cheeseman, G. Scalmani, V. Barone, G. A. Petersson, H. Nakatsuji, X. Li, M. Caricato, A. V. Marenich, J. Bloino, B. G. Janesko, R. Gomperts, B. Mennucci, H. P. Hratchian, J. V. Ortiz, A. F. Izmaylov, J. L. Sonnenberg, D. Williams-Young, F. Ding, F. Lipparini, F. Egidi, J. Goings, B. Peng, A. Petrone, T. Henderson, D. Ranasinghe, V. G. Zakrzewski, J. Gao, N. Rega, G. Zheng, W. Liang, M. Hada, M. Ehara, K. Toyota, R. Fukuda, J. Hasegawa, M. Ishida, T. Nakajima, Y. Honda, O. Kitao, H. Nakai, T. Vreven, K. Throssell, J. A. Montgomery Jr., J. E. Peralta, F. Ogliaro, M. J. Bearpark, J. J. Heyd, E. N. Brothers, K. N. Kudin, V. N. Staroverov, T. A. Keith, R. Kobayashi, J. Normand, K. Raghavachari, A. P. Rendell, J. C. Burant, S. S. Iyengar, J. Tomasi, M. Cossi, J. M. Millam, M. Klene, C. Adamo, R. Cammi, J. W. Ochterski, R. L. Martin, K. Morokuma, O. Farkas, J. B. Foresman and D. J. Fox, *Gaussian 16, Revision B.01*, Wallingford, CT, 2016.
42 N. Keller, D. Bessinger, S. Reuter, M. Calik, L. Ascherl, F. C. Hanusch, F. Auras and T. Bein, *J. Am. Chem. Soc.*, 2017, **139**, 8194–8199.
43 Y.-S. Kim, M. Marsman, G. Kresse, F. Tran and P. Blaha, *Phys. Rev. B: Condens. Matter Mater. Phys.*, 2010, **82**, 205212.
44 D. P. Arnold, R. D. Hartnell, G. A. Heath, L. Newby and R. D. Webster, *Chem. Commun.*, 2002, 754–755, DOI: 10.1039/b200803n.
45 T. Holstein, *Ann. Phys.*, 1959, **8**, 325–342.
46 T. Holstein, *Ann. Phys.*, 1959, **8**, 343–389.
47 R. A. Marcus, *Rev. Mod. Phys.*, 1993, **65**, 599–610.
48 R. E. Peierls, *Quantum theory of solids*, Oxford University Press, 1955.
49 L. Zhu, Y. Yi, Y. Li, E.-G. Kim, V. Coropceanu and J.-L. Brédas, *J. Am. Chem. Soc.*, 2012, **134**, 2340–2347.
50 F. Simone, M. Didier and C. Sergio, *Adv. Funct. Mater.*, 2016, **26**, 2292–2315.
51 Y. Li, Y. Yi, V. Coropceanu and J.-L. Brédas, *Phys. Rev. B: Condens. Matter Mater. Phys.*, 2012, **85**, 245201.
52 X. Qian, H. Liu, C. Huang, S. Chen, L. Zhang, Y. Li, J. Wang and Y. Li, *Sci. Rep.*, 2015, **5**, 7756.
53 J. Bardeen and W. Shockley, *Phys. Rev.*, 1950, **80**, 72–80.
54 G. Schusteritsch, M. Uhrin and C. J. Pickard, *Nano Lett.*, 2016, **16**, 2975–2980.
55 L. Chen, L. Wang, Z. Shuai and D. Beljonne, *J. Phys. Chem. Lett.*, 2013, **4**, 2158–2165.
56 M. Long, L. Tang, D. Wang, Y. Li and Z. Shuai, *ACS Nano*, 2011, **5**, 2593–2600.
57 Y. Jing and T. Heine, *J. Am. Chem. Soc.*, 2019, **141**, 743–747.
58 H. L. Anderson, *Tetrahedron Lett.*, 1992, **33**, 1101–1104.
59 W.-N. Yen, S.-S. Lo, M.-C. Kuo, C.-L. Mai, G.-H. Lee, S.-M. Peng and C.-Y. Yeh, *Org. Lett.*, 2006, **8**, 4239–4242.
60 A. M. Evans, L. R. Parent, N. C. Flanders, R. P. Bisbey, E. Vitaku, M. S. Kirschner, R. D. Schaller, L. X. Chen, N. C. Gianneschi and W. R. Dichtel, *Science*, 2018, **361**, 52–57.
61 G. Baranović, L. Colombo, K. Furić, J. R. Durig, J. F. Sullivan and J. Mink, *J. Mol. Struct.*, 1986, **144**, 53–69.
62 O. G. Reid, D. T. Moore, Z. Li, D. Zhao, Y. Yan, K. Zhu and G. Rumbles, *J. Phys. D: Appl. Phys.*, 2017, **50**, 493002.
63 T. J. Savenije, A. J. Ferguson, N. Kopidakis and G. Rumbles, *J. Phys. Chem. C*, 2013, **117**, 24085–24103.
64 M. J. Bird, O. G. Reid, A. R. Cook, S. Asaoka, Y. Shibano, H. Imahori, G. Rumbles and J. R. Miller, *J. Phys. Chem. C*, 2014, **118**, 6100–6109.
65 P. Prins, F. C. Grozema, J. M. Schins and L. D. A. Siebbeles, *Phys. Status Solidi B*, 2006, **243**, 382–386.
66 O. G. Reid and G. Rumbles, *J. Phys. Chem. Lett.*, 2013, **4**, 2348–2355.
67 O. G. Reid, J. A. N. Malik, G. Latini, S. Dayal, N. Kopidakis, C. Silva, N. Stingelin and G. Rumbles, *J. Polym. Sci., Part B: Polym. Phys.*, 2012, **50**, 27–37.
68 O. G. Reid, R. D. Pensack, Y. Song, G. D. Scholes and G. Rumbles, *Chem. Mater.*, 2014, **26**, 561–575.

